Electrospun P2-type $Na_{2/3}(Fe_{1/2}Mn_{1/2})O_2$ Hierarchical Nanofibers as Cathode Material for Sodium-Ion Batteries

Sujith Kalluri,[†] Kuok Hau Seng,[†] Wei Kong Pang,[†,§] Zaiping Guo,*,[†,‡] Zhixin Chen,[‡] Hua-Kun Liu,[†] and Shi Xue Dou[†]

[†]Institute for Superconducting and Electronic Materials and [‡]School of Mechanical, Materials and Mechatronics Engineering, University of Wollongong, Wollongong, NSW 2500, Australia

[§]Australian Nuclear Science and Technology Organisation, Locked Bag 2001, Kirrawee DC, NSW 2232, Australia

Ⓢ Supporting Information

ABSTRACT: Sodium-ion batteries can be the best alternative to lithium-ion batteries, because of their similar electrochemistry, nontoxicity, and elemental abundance and the low cost of sodium. They still stand in need of better cathodes in terms of their structural and electrochemical aspects. Accordingly, the present study reports the first example of the preparation of $Na_{2/3}(Fe_{1/2}Mn_{1/2})O_2$ hierarchical nanofibers by electrospinning. The nanofibers with aggregated nanocrystallites along the fiber direction have been characterized structurally and electrochemically, resulting in enhanced cyclability when compared to nanoparticles, with initial discharge capacity of ~195 mAh g^{-1}. This is attributed to the good interconnection among the fibers, with well-guided charge transfers and better electrolyte contacts.

KEYWORDS: batteries, sodium, electrospinning, nanofibers, electrochemistry
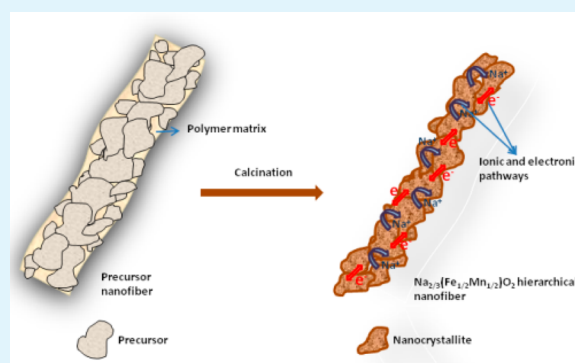
Because of limited energy resources for the future, it is necessary to look for eco-friendly and affordable renewable energy systems and their systematic utilization by safe and facile energy storage systems.[1,2] Because of its superior electrochemistry and cell design, the lithium-ion battery has been predominant in portable applications and could be in electric vehicles, resulting in the depletion of lithium reserves, which is hardly sustainable for future needs.[3] Thus, an alternative that can compete with lithium-ion battery (LIB) technology on the global market is inevitably needed. Sodium is nontoxic and inexpensive, is the next lighter and smaller alkali metal other than lithium, has a redox potential suitable for battery applications (0.3 V *vs* Li), and importantly, is an abundant element, with a similar electrochemistry to that of lithium in LIBs. All these attributes make sodium an alternative to lithium and pave the way for research on feasible sodium-based electrode materials.[4] Surprisingly, the sodium-ion battery (SIB) system is not new; in the 1970s, some researchers conducted early experiments on Na-ion intercalation in certain layered structures,[5,6] although there was little further research because of the commercial dominance of LIBs. Considering the socioeconomic and chemical aspects of sodium, there is a need for a new class of sodium-based cathodes and to achieve further understanding of Na-ion intercalation/deintercalation mechanisms and charge transfers compared with those of the analogous Li materials.

Research on cathode materials for SIBs has been focused on compounds ranging from polyanions to layered transition-metal oxides, and it is suggested that layered sodium transition-metal oxides show outstanding electrode properties.[7,8] Layered sodium metal oxides are classified as O3- and P2-types, based on the location of the Na-ion at octahedral and prismatic sites, respectively, and there are subgroups of new phases such as the new O3 and P'3-phases.[9] The P2-type layered oxides such as $Na_{0.6}MnO_2$ and $Na_{0.7}CoO_2$ show improved initial capacity when compared to those of the O3-type $NaMO_2$ (M = Co, Cr, V, $Ni_{0.5}Mn_{0.5}$, etc.), but with poor cyclability.[10−14] To make progress with such cathodes electrochemically and economically, toxic and costly metals such as Cr and Co are need to be replaced with safe and economical Mn and Fe.[8] Various groups have successfully prepared P2-type $Na_x(Mn_{1−y}Fe_y)O_2$ (x = 2/3, y = 1/2) by solid-state reaction, autocombustion, and sol−gel processes,[15−17] and it delivers an excellent initial discharge capacity of ~190 mAh g^{-1} at a low current density in the voltage range of 1.5−4.3 V with optimized proportions of Mn and Fe. Unfortunately, the cyclability of these materials is limited and needs to be improved for large-scale applications. Apart from doping and surface engineering of active materials, nanostructured design of electrodes and electrolyte compositions can contribute to the overall performance of batteries.[18] Nanomaterials have a short Na-ion diffusion distance, relatively

less volume expansion during cycling, and better electrolyte contacts due to their high specific surface area, all of which are responsible for improved electrochemical performance in SIBs.[19,20] Nanoparticles have a regular tendency to self-aggregate because of their high surface energy; however, this results in limited contact with the conducting components, which leads to declining net battery performance. Such self-aggregation can be mitigated by one-dimensional (1D) nanostructures, which could have better contact areas with the electrolyte and offer improved electrochemistry and cycle life.[21,22] Feasible and reliable fabrication techniques are essential for 1D nanostructures. Electrospinning is a low-cost, large-scale, and facile one-pot synthesis technique for continuous nanofibers, and such nanofibrous electrodes offer high porosity, good interfacial contact, and well-guided charge transfer toward the current collector.[23−26]

There have been no reports to date on 1D nanofibrous sodium metal oxide cathodes for SIBs. We have now successfully fabricated electrospun nanofibers of P2-type $Na_{2/3}(Fe_{1/2}Mn_{1/2})O_2$ material and characterized them structurally and electrochemically, demonstrating improved cyclability with better structural stability. We have also attempted to understand the correlation between 1D nanofibers and electrochemical performance.

$Na_{2/3}(Fe_{1/2}Mn_{1/2})O_2$ nanofibers and nanoparticles were prepared by electrospinning and the sol−gel process, respectively and hereafter are designated as NFMO NF and NFMO NP, respectively. Detailed synthesis procedures are explained in the Supporting Information. X-ray diffraction (XRD) patterns for both samples prepared at 900 °C are shown in Figure 1. Both patterns appear the same, with well-
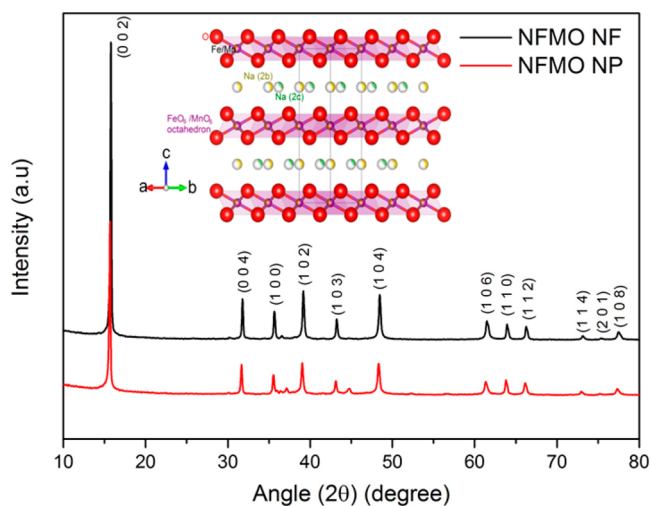

Figure 1. XRD patterns of NFMO NF and NFMO NP (inset: crystal structure of P2-type NFMO).

crystallized sharp reflections associated with the hexagonal phase system and space group $P63/mmc$, which are consistent with the literature.[15−17] NFMO is a P2-type structure, with the Na-ions accommodated at two locations in prismatic sites and stacked in between the ordered hybrid octahedral layers of FeO_6 and MnO_6 (inset of Figure 1).

Figure 2a shows an scanning electron microscope (SEM) image of the as-spun precursor fibers with average diameter of ~400 nm (see also Figure S1a in the Supporting Information). After calcination, the polyvinylpyrrolidone (PVP) and organic

residues are sublimated, resulting in NFMO NF (Figure 2b), with average diameter of ~170 nm (see Figure S1b in the Supporting Information). Figure S2 in the Supporting Information shows an SEM image of NFMO NP with average particle size of ~500 nm. High-resolution transmission electron microscope (HR-TEM) images were obtained to determine the crystallinity and secondary structure of the hierarchical nanofibers. Figure 2c is in good agreement with the SEM image in terms of its 1D morphology. Notably, the NFMO nanocrystallites are tightly connected with each other within the nanofiber (as highlighted with contours in Figure 2c), and the self-aggregation of nanocrystallites is greatly reduced due to the attachment of nanocrystallites in the nanofiber. Figure 2d shows a high-resolution TEM image of the well-developed nanocrystallite taken at the diffraction condition near the zone axis $[\bar{1}100]$. It shows that the width of the lattice fringes is about 5.4 Å, as marked in Figure 2d, which is in good agreement with the XRD data and corresponding to the (0 0 2) plane of the hexagonal structure. The longitudinal direction is along $[11\bar{2}0]$. Figure 2f presents the energy-dispersive X-ray (EDX) spectrum of NFMO NF with the individual elements Na, Fe, Mn, and O.

The electrochemical properties were examined for both samples from charge−discharge curves and cyclic voltammograms (CVs) using a battery analyzer and an electrochemical workstation in the voltage range of 1.5−4.2 V. Figure 3a shows the charge−discharge behavior in the initial cycle and the 80th cycle for both samples at 0.1 C current rate (1 C = 260 mA g^{-1}). The charge−discharge curves show similar behavior to that reported elsewhere, with two plateaus at 4 and 3.4 V, corresponding to phase transitions from P2-type to O2-type with OP4-type as an intermediate phase. The additional plateau around 2.1 V could be attributed to reverse phase transition from OP4-type to P2-type during discharge.[15] Interestingly, NFMO NF showed an improved initial discharge capacity of ~195 mAh g^{-1} when compared to that of NFMO NP (~179 mAh g^{-1}). Under the same specifications at the 80th cycle, the discharge capacity is ~167 mAh g^{-1} and ~113 mAh g^{-1} for NFMO NF and NP, respectively, and it is apparent that there is a notable impact of morphology on the stability of NFMO during cycling. Thus, cyclability was evaluated over 80 cycles at the 0.1 C rate, in which the NFMO NF showed an initial capacity decay from ~195 mAh g^{-1} to ~175 mAh g^{-1} for the first few cycles (which could be due to the inherent internal resistance of the cell and the conducting nature of NFMO[27]) and thereafter maintained excellent cyclability [Figure 3(b)], with discharge capacity of ~166 mAh g^{-1} after 80 cycles with 86.4% capacity retention, which is a significant improvement when compared to that of the NP (60.5% capacity retention with the discharge capacity of ~113 mAh g^{-1}). The enhanced capacity and cyclability could be attributed to the well-guided charge transfer kinetics and better wettability of the well-interconnected and highly porous nanofibrous network with respect to the electrolyte over cycling, whereas the NP sample delivered relatively poor capacity retention, which could be attributed to pulverization of the material, less contact of the active material with the electrolyte due to possible self-aggregation of nanoparticles over cycling, and also the relatively larger crystallite size. Such self-aggregation is barely seen for the nanofibers because of the hierarchical crystallite formation at localized sites along the fiber structure during the calcination, which reduces the diffusion in the sintering process.[23] In addition, capacity fade can be observed for the NP sample from

8954

dx.doi.org/10.1021/am502343s | ACS Appl. Mater. Interfaces 2014, 6, 8953−8958
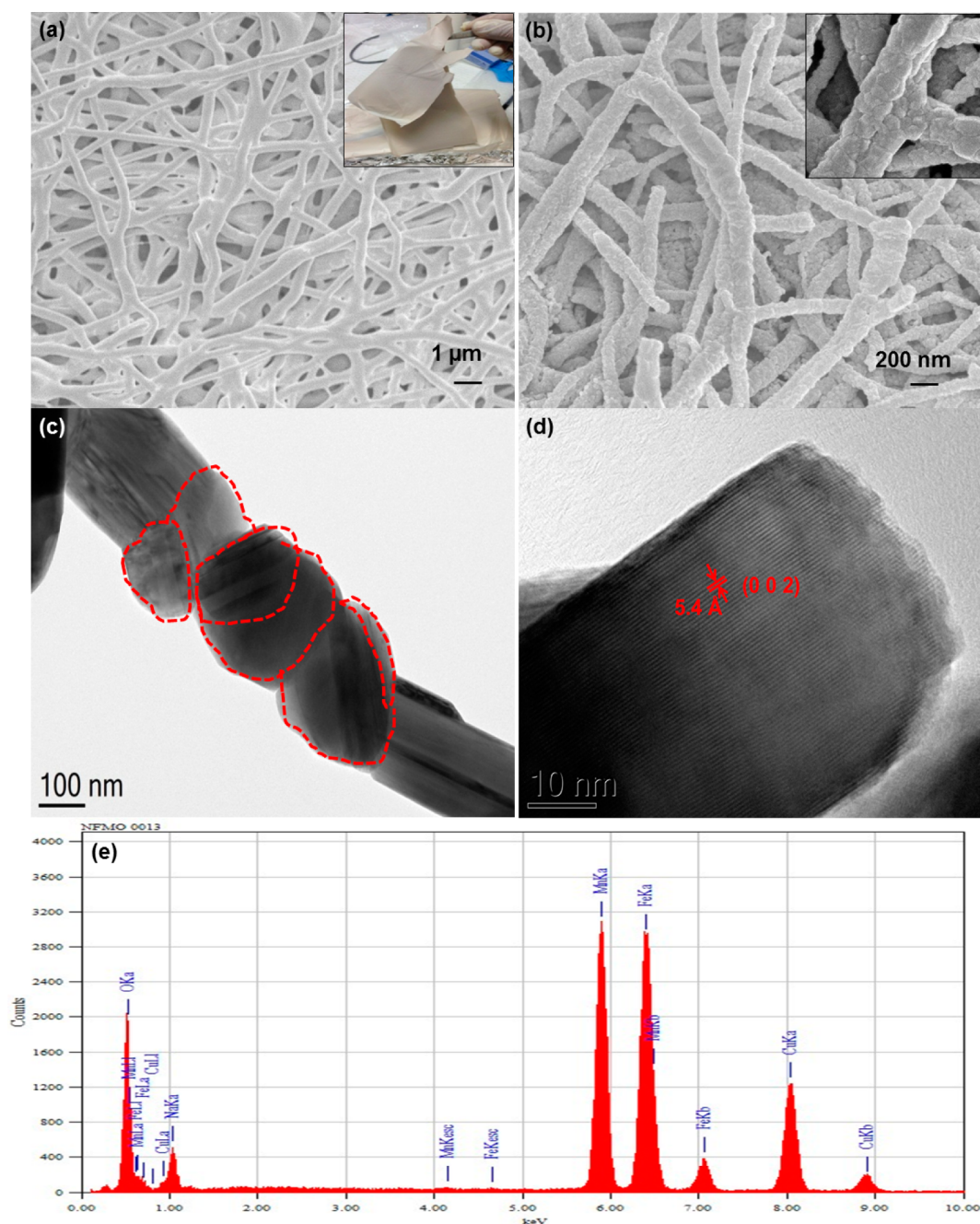
Figure 2. SEM images of (a) as-spun nanofibers (inset: photograph of as-spun nanofibrous mat), and (b) NFMO nanofibers (inset: high-resolution image); (c) HR-TEM image of NFMO nanofiber with hierarchical arrangement of nanocrystallites; (d) high-resolution TEM image of a longitudinal nanoparticle taken from near the zone axis $[\bar{1}100]$ showing fringes of (0 0 2) and the longitudinal direction of the particle is $[11\bar{2}0]$; and (e) EDX spectrum.

the initial cycle to the final cycle, which may be due to the volumetric expansion of the material during repeated Na-ion intercalation/deintercalation processes during cycling and loss of electrical contact between the active material and the current collector.

To understand the impact of morphology on rate performance, we characterized both samples at various rates from 0.1 to 15 C. The NFMO NF samples featured slightly improved rate performance when compared to NFMO NP. At the high current rates of 1 C, 2 C, and 5 C, the NFMO NF sample showed good discharge capacity values when compared to NFMO NP (see Figure 3c). This is attributed to the minimal

polarization of the NF electrodes when compared to the NP ones. At the very high rates of 10 and 15 C for both samples, however, the discharge capacity values are dramatically diminished to the range of 33−70 mAh g^{-1}. The charge−discharge curves of both electrodes at various current rates from 0.1 C to 15 C (see Figure S3a, b in the Supporting Information), reveal that with increasing rate, the two voltage plateaus at 4 and 3.4 V are gradually diminishing, which could be attributed to the polarization of the electrodes, hindering reversible phase transitions from P2-type to O2-type and leading to corresponding deterioration in the crystal structure of the active material, thereby decreasing Na-ion intercalation/
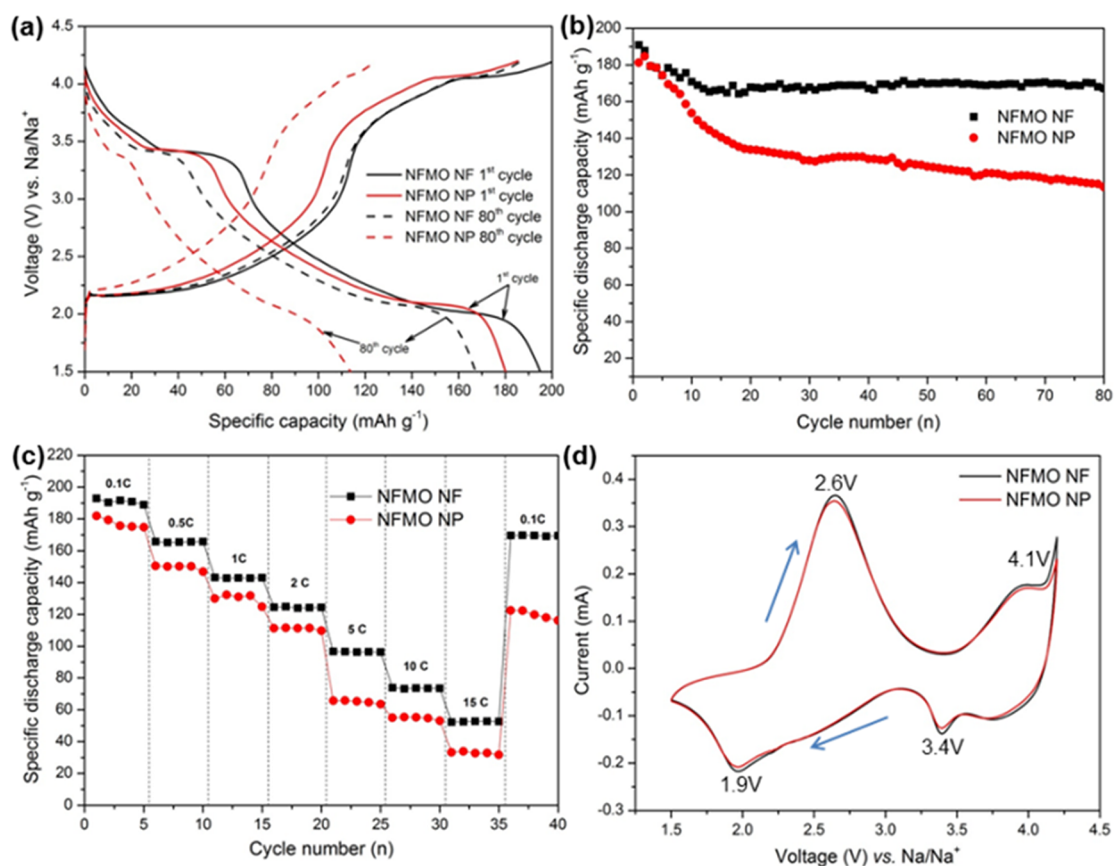
Figure 3. (a) Charge−discharge curves of NFMO NF and NP at the initial and 80th cycles at the 0.1 C current rate; (b) corresponding cycling stability; (c) rate performance; and (d) cyclic voltammograms of NFMO NF and NP at the scan rate of 0.1 mV s^{-1}. The voltage range is 1.5−4.2 V.

deintercalation reactions.[8] These reactions are further confirmed by the CVs (Figure 3d), with Na as reference and counter electrode in the voltage range of 1.5−4.2 V at the scan rate of 0.1 mV s^{-1}. Two pairs of peaks are observed in both the anodic and cathodic sweeps at 2.6 vs 1.9 V and 4.1 vs 3.4 V, corresponding to redox reactions of Mn^{3+}/Mn^{4+} and Fe^{3+}/Fe^{4+}, respectively.[28,29] The phase transition from quasi-reversible P2-type to O2-type due to less Na content upon extraction corresponds to the anodic peak at 4.1 V. This phase change is associated with slight oxygen layer dislocation in the crystal structure of NFMO, resulting in octahedral phase. During reduction, the octahedral phase is converted back to hexagonal phase.[29,8] These voltage plateaus associated with phase transitions are in good agreement with the corresponding charge−discharge curves.

Various reasons are proposed for the improved electrochemical performance of the NFMO NF over that of NFMO NP. During the calcination of the as-spun nanofibers, NFMO nanocrystallites are formed at localized sites along the direction of fiber growth (schematic illustration in Figure 4a), which is also evident from HR-TEM and SEM analyses (see Figure 3b, c). Such hierarchical growth of nanofibers thereby prevents sintering and self-aggregation,[23,30] whereas nanoparticles without a well-defined morphology have a tendency to self-aggregate, as shown in Figure 4b. Thus, 1D NFMO nanofibers take advantage of their large effective contact area and consequent better wettability with the electrolyte during cycling, which significantly contributes to improved performance. In addition, the charge transfer kinetics in the active material also influences the electrochemical conductivity.

NFMO NFs display well-guided transport behavior, with long mean free paths of charge carriers (Na-ions and electrons), as shown in Figure 4a, which improves the electronic and ionic conductivities. The proposed mechanism is evident from the electrochemical impedance spectroscopy (EIS) studies and ex $situ$ SEM analysis, as shown in Figures S4a, b and S5a, b in the Supporting Information, respectively. EIS measurements were performed to understand the conductivity profiles of the NFs and NPs. The Nyquist plots present the lower charge transfer resistance of 47 Ω for NFMO NF when compared to that of NFMO NP (140 Ω) before cycling, and the same trend is followed even after 80 cycles. Ex $situ$ SEM analysis of both electrodes after 40 cycles revealed the excellent structural stability with well-defined hierarchical structure of the NFs and the self-agglomeration of NPs, as shown in Figure S5 in the Supporting Information. Further studies relating to the improvement of rate performance at very high current rates and understanding the interfacial properties need to be conducted.

To summarize, structurally stable P2-type $Na_{2/3}(Fe_{1/2}Mn_{1/2})O_2$ hierarchical nanofibers were fabricated by electrospinning. The hierarchical arrangement is formed during the calcination from ordered stacking of nanocrystallites along the direction of fiber growth. These nanofibers showed enhanced electrochemical performance in SIBs, with an initial discharge capacity of ∼195 mAh g^{-1} and improved cyclability with a capacity retention of 86.4% over 80 cycles. These hierarchical structures are unique in terms of being well-interconnected for charge conductivity and well-guided
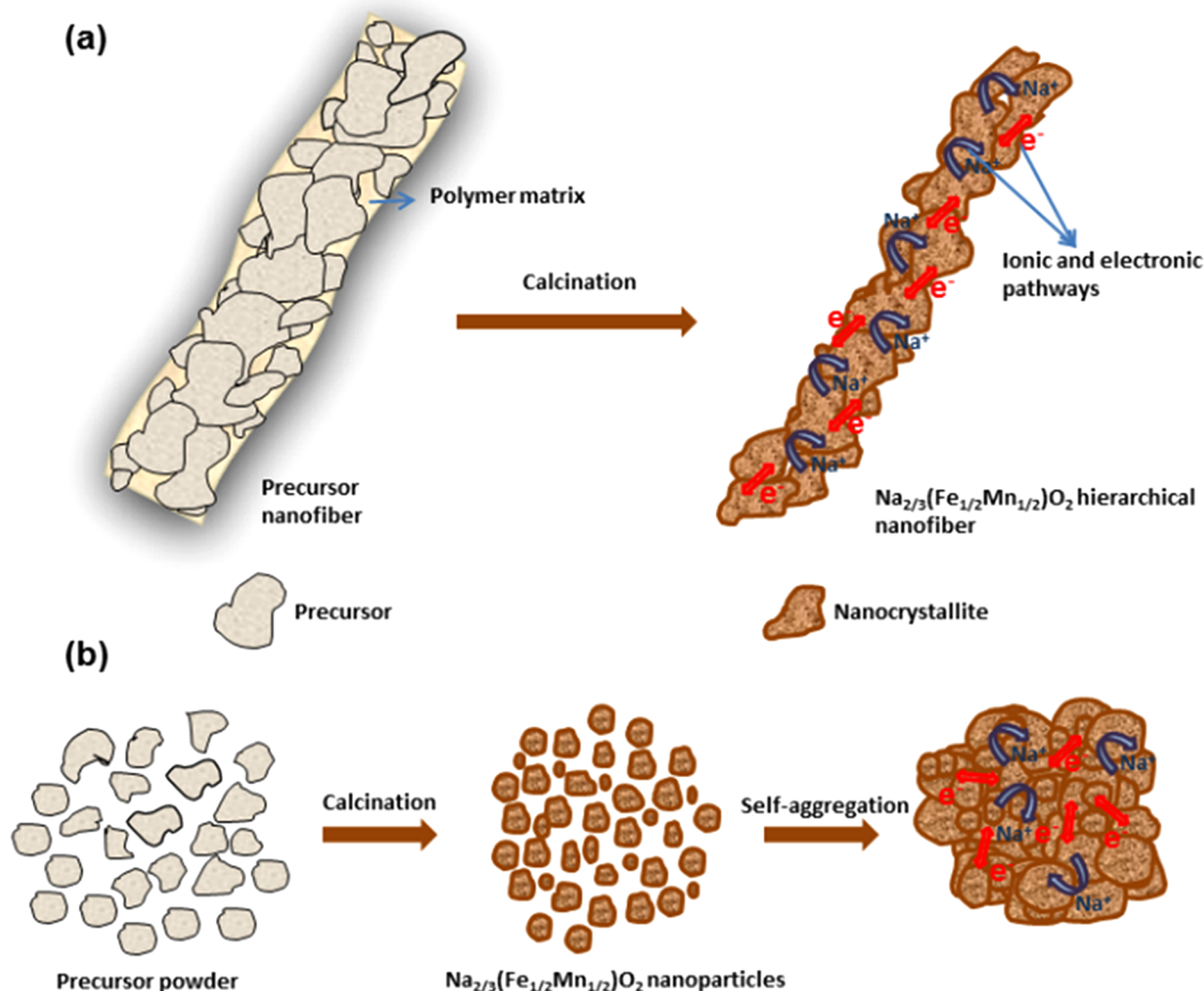
Figure 4. Formation mechanism and charge transfer pathways in (a) hierarchical NFMO NF and (b) NFMO NP.

diffusion pathways. Such hierarchical nanofibers could be one of the potential cathode candidates for SIBs.

ASSOCIATED CONTENT

Ⓢ Supporting Information

Experimental section with characterization techniques, fiber diameter, and particle size distributions of NFMO NF and NP, respectively, with an SEM image of NFMO NP. It also includes the charge−discharge behavior of NFMO NF and NP at various rates, electrochemical impedance plots, and *ex situ* SEM images of NFMO NF and NP after 40 cycles. This material is available free of charge via the Internet at http://pubs.acs.org.

AUTHOR INFORMATION

Corresponding Author

*E-mail: zguo@uow.edu.au.

Notes

The authors declare no competing financial interest.

ACKNOWLEDGMENTS

REFERENCES

(1) Pan, H.; Hu, Y. S.; Chen, L. Room-temperature Stationary Sodium-ion Batteries for Large-scale Electric Energy Storage. *Energy Environ. Sci.* **2013**, *6*, 2338−2360.

(2) Dunn, B.; Kamanth, H.; Tarascon, J. M. Electrical Energy Storage for the Grid: A Battery of Choices. *Science* **2011**, *334*, 928−935.

(3) Tarascon, J. M.; Armand, M. Issues and Challenges Facing Rechargeable Lithium Batteries. *Nature* **2001**, *414*, 359−367.

(4) Slater, M. D.; Kim, D.; Lee, E.; Johnson, C. S. Sodium-Ion Batteries. *Adv. Funct. Mater.* **2013**, *23*, 947−958.

(5) Paranat, J. P.; Olazcuag, R.; Devalett, M.; Fouassie, C.; Hagenmuller, P. Sur quelques Nouvelles Phases de Formule Na_xMnO_2 ($x \leq 1$). *J. Solid State Chem.* **1971**, *3*, 1−5.

(6) Whittingham, M. S. Chemistry of Intercalation Compounds: Metal Guests in Chalcogenide Hosts. *Prog. Solid State Chem.* **1978**, *12*, 41−99.

(7) Masquelier, C.; Croguennec, L. Polyanionic (Phosphates, Silicates, Sulfates) Frameworks as Electrode Materials for Rechargeable Li (or Na) Batteries. *Chem. Rev.* **2013**, *113*, 6552−6591.

(8) Buchholz, D.; Chagas, L. G.; Winter, M.; Passerini, S. P2-type Layered $Na_{0.45}Ni_{0.22}Co_{0.11}Mn_{0.66}O_2$ as Intercalation Host Material for Lithium and Sodium Batteries. *Electrochim. Acta* **2013**, *110*, 208−213.

(9) Yoncheva, M.; Stoyanova, R.; Zhecheva, E.; Kuzmanova, E.; Vassileva, M. S.; Nihtianova, D.; Carlier, D.; Guignard, M.; Delmas, C. Structure and Reversible Lithium Intercalation in a New P′3-phase: $Na_{2/3}Mn_{1-y}Fe_yO_2$ (y = 0, 1/3, 2/3). *J. Mater. Chem.* **2012**, *22*, 23418−23427.

8957

dx.doi.org/10.1021/am502343s | *ACS Appl. Mater. Interfaces* 2014, 6, 8953−8958

(10) Komaba, S.; Takei, C.; Nakayama, T.; Ogata, A.; Yabuuchi, N. Electrochemical Intercalation Activity of Layered $NaCrO_2$ vs $LiCrO_2$. *Electrochem. Commun.* **2010**, *12*, 355−358.

(11) Komaba, S.; Murata, W.; Ishikawa, T.; Yabuuchi, N.; Ozeki, T.; Nakayama, T.; Ogata, A.; Gotoh, K.; Fujiwara, K. Electrochemical Na Insertion and Solid Electrolyte Interphase for Hard-Carbon Electrodes and Application to Na-Ion Batteries. *Adv. Funct. Mater.* **2011**, *21*, 3859−3867.

(12) Delmas, C.; Braconnier, J. J.; Fouassier, C.; Hagenmuller, P. Electrochemical Intercalation of Sodium in Na_xCoO_2 bronzes. *Solid State Ionics.* **1981**, *3−4*, 165−169.

(13) Berthelot, R.; Carlier, D.; Delmas, C. Electrochemical Investigation of the P2-Na_xCoO_2 Phase Diagram. *Nat. Mater.* **2011**, *10*, 74−80.

(14) Lu, Z.; Dahn, J. R. In Situ X-Ray Diffraction Study of P 2 $Na_{2/3}[Ni_{1/3}Mn_{2/3}]O_2$. *J. Electrochem. Soc.* **2001**, *148*, A1225−A1229.

(15) Yabuuchi, N.; Kajiyama, M.; Iwatate, J.; Nishikawa, H.; Hitomi, S.; Okuyama, R.; Usui, R.; Yamada, Y.; Komaba, S. P2-type $Na_x[Fe_{1/2}Mn_{1/2}]O_2$ made from Earth-Abundant Elements for Rechargeable Na Batteries. *Nat. Mater.* **2012**, *11*, 512−517.

(16) Mortemard de Boisse, B.; Carlier, D.; Guignard, M.; Delmas, C. Structural and Electrochemical Characterizations of P2 and New O3-$Na_xMn_{1-y}Fe_yO_2$ Phases Prepared by Auto-Combustion Synthesis for Na-Ion Batteries. *J. Electrochem. Soc.* **2013**, *160*, A569−A574.

(17) Xu, J.; Chou, S. L.; Wang, J. L.; Liu, H. K.; Dou, S. X. Layered P2-$Na_{0.66}Fe_{0.5}Mn_{0.5}O_2$ Cathode Material for Rechargeable Sodium-Ion Batteries. *ChemElectroChem.* **2014**, *1*, 371−374.

(18) Zhou, S.; Wang, D. Unique Lithiation and Delithiation Processes of Nanostructured Metal Silicides. *ACS Nano* **2010**, *4*, 7014−7020.

(19) Chan, C. K.; Peng, H.; Liu, G.; Mcilwrath, K.; Zhang, X. F.; Huggins, R. A.; Cui, Y. High-Performance Lithium Battery Anodes Using Silicon Nanowires. *Nat. Nanotechnol.* **2008**, *3*, 31−35.

(20) Liu, J.; Xia, H.; Xue, D.; Lu, L. Double-Shelled Nanocapsules of V_2O_5-Based Composites as High-Performance Anode and Cathode Materials for Li Ion Batteries. *J. Am. Chem. Soc.* **2009**, *131*, 12086−12087.

(21) Brezesinski, T.; Wang, J.; Tolbert, S. H.; Dunn, B. Ordered Mesoporous R-MoO_3 with Iso-oriented Nanocrystalline Walls for Thin-Film Pseudocapacitors. *Nat. Mater.* **2010**, *9*, 146−151.

(22) Ge, J.; Zhang, Q.; Zhang, T.; Yin, Y. Core-Satellite Nanocomposite Catalysts Protected by a Porous Silica Shell: Controllable Reactivity, High Stability, and Magnetic Recyclability. *Angew. Chem., Int. Ed.* **2008**, *47*, 8924−8928.

(23) Hagen, R.; Lepcha, A.; Song, X.; Tyrra, W.; Mathur, S. Influence of Electrode Design on the Electrochemical Performance of $Li_3V_2(PO_4)_3$/C Nanocomposite Cathode in Lithium Ion Batteries. *Nano Energy* **2013**, *2*, 304−313.

(24) Thavasi, V.; Singh, G.; Ramakrishna, S. Electrospun Nanofibers in Energy and Environmental Applications. *Energy Environ. Sci.* **2008**, *1*, 205−221.

(25) Kalluri, S.; Seng, K. H.; Guo, Z.; Liu, H. K.; Dou, S. X. Electrospun Lithium Metal Oxide Cathode Materials for Lithium-ion Batteries. *RSC Adv.* **2013**, *3*, 25576−25601.

(26) Denton, A. R.; Ashcroft, N. W. Vegard's Law. *Phys. Rev. A* **1991**, *43*, 3161−3164.

(27) Liu, G.; Xun, S.; Vukmirovic, N.; Song, X.; Velasco, P. O.; Zheng, H.; Battaglia, V. S.; Wang, L.; Yang, W. Polymers with Tailored Electronic Structure for High Capacity Lithium Battery Electrodes. *Adv. Mater.* **2011**, *23*, 4679−4683.

(28) Yuan, D.; Hu, X.; Qian, J.; Pei, F.; Wu, F.; Mao, R.; Ai, X.; Yang, H.; Cao, Y. P2-type $Na_{0.67}Mn_{0.65}Fe_{0.2}Ni_{0.15}O_2$ Cathode Material with High-capacity for Sodium-ion Battery. *Electrochim. Acta* **2014**, *116*, 300−305.

(29) Thorne, J. S.; Dunlap, R. A.; Obrovac, M. N. Structure and Electrochemistry of $Na_xFe_xMn_{1-x}O_2$ $(1.0 \leq x \leq 0.5)$ for Na-Ion Battery Positive Electrodes. *J. Electrochem. Soc.* **2013**, *160*, A361−A367.

(30) Mai, L.; Xu, L.; Han, C.; Xu, X.; Luo, Y.; Zhao, S.; Zhao, Y. Electrospun Ultralong Hierarchical Vanadium Oxide Nanowires with High Performance for Lithium Ion Batteries. *Nano Lett.* **2010**, *10*, 4750−4755.

8958

dx.doi.org/10.1021/am502343s | *ACS Appl. Mater. Interfaces* 2014, 6, 8953−8958